

# Quantifying Non-circular Streaming Motions in Disc Galaxies

J. A. Sellwood<sup>1\*</sup> and Ricardo Zánmar Sánchez<sup>1,2†</sup>

<sup>1</sup>*Rutgers University, Department of Physics & Astronomy, 136 Frelinghuysen Road, Piscataway, NJ 08854-8019, USA*

<sup>2</sup>*INAF – Osservatorio Astrofisico di Catania, Via Santa Sofia 78, I-95123 Catania, Italy*

13 August 2018

## ABSTRACT

High-quality velocity maps of galaxies frequently exhibit signatures of non-circular streaming motions. We here apply the software tool, *velfit* recently proposed by Spekkens & Sellwood, to five representative galaxies from the THINGS sample. We describe the strengths and weaknesses of the tool, and show that it is both more powerful and yields results that are more easily interpreted than the commonly used procedure. We demonstrate that it can estimate the magnitudes of forced non-circular motions over a broad range of bar strengths from a strongly barred galaxy, through cases of mild bar-like distortions to placing bounds on the shapes of halos in galaxies having extended rotation curves. We identify mild oval distortions in the inner parts of two dwarf galaxies, NGC 2976 and NGC 7793, and show that the true strength of the non-axisymmetric gas flow in the strongly barred galaxy NGC 2903 is revealed more clearly in our fit to an optical H $\alpha$  map than to the neutral hydrogen data. The method can also yield a direct estimate of the ellipticity of a slowly-rotating potential distortion in the flat part of a rotation curve, and we use our results to place tight bounds on the possible ellipticity of the outer halos of NGC 3198 and NGC 2403.

**Key words:** galaxies: haloes – galaxies: kinematics and dynamics – galaxies: spiral – galaxies: structure – methods: data analysis

## 1 INTRODUCTION

The centrifugal balance of gas on near circular orbits in a galaxy yields a direct estimate of the central attraction, which is the first step towards a model for the mass distribution. The estimation of galaxy rotation curves therefore has a long history (see Sofue & Rubin 2001, for a review).

Well-sampled 2D velocity maps provide sufficient information to identify the rotation centre and to test whether the line-of-sight velocity field is, or is not, consistent with a circular flow pattern in an inclined plane about a common rotation centre. The widely-used software utility *rotcur* (Begeman 1987) divides the velocity map into a number of elliptical elements that are assumed to be projected circles around which the gas moves on circular orbits. It yields an estimate of the circular speed in each annulus, and has options to fit for, or hold fixed, the rotation centre, systemic velocity, position angle and inclination in each annulus. It is uniquely powerful in its ability to extract information when the gas layer is warped.

A number of possible systematic errors in the

fitted velocity have been discussed. Beam smearing (van den Bosch & Swaters 2001) is obviously reduced by improved spatial resolution of the observations, *e.g.*, by using optical data when available. Various forms of turbulence – also described as pressure support or as an asymmetric drift (Valenzuela *et al.* 2007) – can be recognized and corrected for in high quality data (Oh *et al.* 2008).

The present paper addresses the systematic error caused by non-circular flow patterns. Velocity “wiggles” or larger-scale distortions of the isovelocity contours have long been recognized (*e.g.* Bosma 1978) in well-sampled 2D velocity maps. Both Hayashi & Navarro (2006) and Valenzuela *et al.* (2007) show qualitatively that non-circular streaming in non-axisymmetric potentials can lead to a mis-estimation of the central attraction. Note that Weiner *et al.* (2001), Kranz *et al.* (2003), Pérez *et al.* (2004) and Weiner (2004) had previously published a number of quantitative models of non-circular flows that took this effect into account; these papers used the additional information contained in the non-circular motions of strongly barred or spiral galaxies to separate the central attractions of the disc and halo.

Not only do non-circular motions arise from bars and other visible distortions, but they may also be caused by expected asphericities in dark matter halos (*e.g.* Jing & Suto

\* E-mail: sellwood@physics.rutgers.edu

† E-mail: zanmar@oact.inaf.it

2002; Allgood *et al.* 2006; Hayashi *et al.* 2007). Because halos are largely pressure-supported, the principal axes of such distortions can slew only slowly with radius, and should appear approximately straight over a moderate radial range. Even though halo shapes are expected to be made rounder by disk formation (*e.g.* Dubinski 1994; Debattista *et al.* 2008), gas in the outer discs is predicted to flow in an elliptical streaming pattern in response to forcing by a non-axisymmetric halo. Hayashi & Navarro (2006) argue that halo-driven non-axisymmetric streaming motions in the inner disc may mask a central cusp in the halo density.

It is therefore desirable to be able to identify non-circular streaming motions in high-quality 2D velocity maps and to correct for their influence when deriving an estimate of the average central attraction. The powerful approach developed by Weiner *et al.* (2001) (see also Zánmar Sánchez *et al.* 2008) requires multiple datasets and is time-consuming to implement. Thus there is a clear need for versatile tool for routine use.

The procedure proposed by Schoenmakers *et al.* (1997) and Schoenmakers (1999) estimates the magnitude of non-circular motions, but does not correct for them. It is embodied in the tool *resuri*, which is an extension of *rotcur*, that has been used quite extensively. More recently Spekkens & Sellwood (2007, hereafter SS07) proposed an alternative tool, *velfit*, that does provide an improved estimate of the mean orbital speed. Here we demonstrate the superior performance of *velfit* by direct comparison of the results from several galaxies. We have chosen to make this comparison using a few galaxies from the THINGS (Walter *et al.* 2008) sample, for which non-circular motions have recently been estimated using *resuri* by Trachternach *et al.* (2008, hereafter TBWBK). In addition, we show that *velfit* can also be applied to optical data from a strongly barred galaxy in the BH $\alpha$ Bar (Hernandez *et al.* 2005) galaxy sample.

## 2 ESTIMATING NON-CIRCULAR MOTIONS

In this section, we describe and compare the two separate software tools that are available for estimating the magnitudes of non-circular flows.

The procedure proposed by Schoenmakers *et al.* (1997), embodied in the tool *resuri*, is an extension of *rotcur* to include an harmonic analysis of the line-of-sight velocities around each ring. These authors use epicycle theory to interpret the fitted non-axisymmetric coefficients, and relate small values to the magnitude of the potential distortion.

It should be noted that non-circular motions are readily confused with the kinematic signature of a warp, since both cause variations in the ellipticity and position angle of the flow pattern.<sup>1</sup> Thus, if the projection geometry is allowed to vary from ring to ring, then a large part of the actual non-circular motion may be masked by radial variations in the position angle (PA) and inclination (*i*). Thus most users (*e.g.* Fathi *et al.* 2005; van Eymeren *et al.* 2009) advocate

<sup>1</sup> In fact, the kinematic signatures of an oval potential and a warp are degenerate only when the principal axis of the potential coincides with either the major or minor axis of the projection (Pence & Blackman 1984; Franx, van Gorkom & de Zeeuw 1994).

constraining *i* & PA to have the same values at all radii. On the other hand, TBWBK justified allowing individual tilts for rings in all the THINGS galaxies from the fact that the magnitudes of non-circular streaming motions in two galaxies (NGC 3198 & DDO 154) were little changed when *i* & PA were allowed to vary compared with when they were constrained to be constant with radius. Here we show that allowing rings to tilt independently led them to miss non-axisymmetric distortions in at least two galaxies: NGC 2976 & NGC 7793.

The tool *resuri* has a number of disadvantages.

(i) A  $\cos(m\theta)$  component in the projected velocities can arise from both  $\cos[(m \pm 1)\theta]$  distortions to the potential (Schoenmakers *et al.* 1997, see also SS07 and references therein), complicating the interpretation of the results.

(ii) It assumes the perturbed velocities are small, and is therefore inadequate to characterize strongly non-axisymmetric flows.

(iii) It makes no correction for the presence of non-circular motions. As a result, the estimated circular speed,  $V_c(R)$ , is biased toward the value of the azimuthal speed on the major axis of the projection, as explained below.

(iv) It treats each ring independently, implying that a mild distortion that is coherent over a significant radial range is more easily masked by noise.

(v) An estimate of the strength of the mild potential distortion responsible for the detected non-axisymmetric flow requires an undesirable difference between two of the fitted coefficients, a consequence of point (i) above, and also includes the sine of an angle whose value cannot be determined from this approach.

SS07 therefore proposed an alternative tool, *velfit* illustrated in Fig. 1.<sup>2</sup> It differs at root by postulating a specific model of the flow that includes a possible non-circular streaming pattern about a fixed direction in the disc plane, *i.e.*, a distortion that has no spirality.

In particular, SS07 assume a flat disc plane and a distortion having a fixed orientation at all radii, although its amplitude may vary with *R*. The tool *velfit* then fits the projected model velocity at a general point (eq. 5 of SS07):

$$V_{\text{model}} = V_{\text{sys}} + \sin i \left[ \bar{V}_t \cos \theta - V_{m,t} \cos m(\theta - \phi_b) \cos \theta - V_{m,r} \sin m(\theta - \phi_b) \sin \theta \right], \quad (1)$$

to derive  $\bar{V}_t(R)$ ,  $V_{m,t}(R)$ ,  $V_{m,r}(R)$ , the angle  $\phi_b$ , the systemic velocity  $V_{\text{sys}}$ , and *i* & PA. (The various quantities are defined in the caption to Fig. 1, which illustrates an elliptical streaming pattern for which  $m = 2$ .)

The code fits a model by minimizing the usual function

$$\chi^2 = \sum_{n=1}^N \left( \frac{V_{\text{obs}}(x, y) - \sum_{k=1}^K w_{k,n} V_k}{\sigma_n} \right)^2. \quad (2)$$

Here  $V_{\text{obs}}(x, y)$  and  $\sigma_n$  are respectively the value of the observed velocity and its uncertainty for the *n*-th pixel at the position (*x, y*) on the sky. The index *k* ranges over *K*, which is the total all three sets of velocities,  $V_k$ , that define

<sup>2</sup> The *velfit* software is publicly available from <http://www.physics.rutgers.edu/~spekkens/velfit/>.

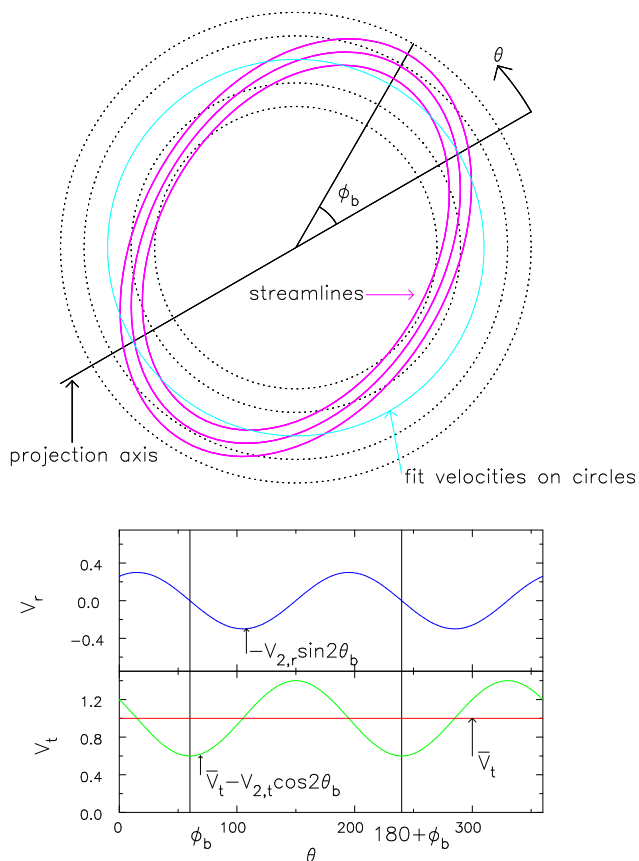


**Figure 1.** A schematic illustration of the approach taken by Spekkens & Sellwood (2007). The magenta lines in the upper panel indicate non-circular streamlines in the disc plane, which is shown face-on. The galaxy is observed in projection, with the intersection of the sky-plane and the disc plane making an angle  $\phi_b$  to the major axis of the elliptical streamlines. Our model of the flow consists of a set of values for  $\bar{V}_t$ ,  $V_{2,t}$  and  $V_{2,r}$  around rings (dotted) at fixed radii. We project the model and fit to the observed data, using linear interpolation to predict data values between rings.

The lower panels illustrate the bisymmetric variations of the radial and azimuthal model velocities (arbitrary scale) in the disc plane around the cyan circle in the upper panel. The radial velocity (blue) varies with angle  $\theta_b = \theta - \phi_b$  to the major axis of the elliptical streaming pattern as  $-V_{2,r} \sin 2\theta_b$ . The azimuthal velocity (green) varies as  $-V_{2,t} \cos 2\theta_b$  about the mean ( $\bar{V}_t$  shown in red). This physically-motivated phase difference between the two non-axisymmetric components is embodied in the fit.

the model velocity (eq. 1) around each of the ellipses. The weights  $w_{k,n}$ , which include the trigonometric factors, also define the interpolation scheme that yields a model prediction at the projected position  $(x, y)$ . The code allows the radial extent of the distortion to be restricted, if desired, while a simple axisymmetric flow is fitted over the remainder of the data. SS07 describe the algorithm in detail.

We here use the term “bar model” to denote any straight bisymmetric distortion no matter what its origin or amplitude. Fig. 1 should not, however, be interpreted to imply that the code can fit only bars, or oval features, although that is its most useful application. The same code

can be used to fit models having higher or lower rotational symmetry,  $m$ , or axisymmetric ( $m = 0$ ) radial flows.

This tool avoids the above-listed disadvantages of the method devised by Schoenmakers *et al.* (1997), as follows.

(i) Fitting a specific distorted flow model to the projected data avoids the complications caused by the coupling of different angular periodicities.

(ii) It can fit for arbitrarily large distortions because it does not require  $V_{m,t}(R)$  &  $V_{m,r}(R)$  to be related by the epicycle approximation.

(iii) It yields  $\bar{V}_t$ , which is an improved estimate of the average orbital speed at each radius, as discussed below.

(iv) It uses all the data in a single fit, making it easier to identify coherent mild distortions in noisy data and to go some way towards “averaging over” small-scale spiral streaming.

(v) The magnitude of a mild potential distortion is much more directly related to the fitted velocity coefficients, as we show in section 3.

An elliptical flow pattern is clearly an idealization. It is a first-order improvement that captures the essential large-scale features of a bar-like flow, and will therefore be a better fit than a flat, axisymmetric model. It does not attempt to include other features, such as shocks in the bar, spiral arms, turbulence, warps, *etc.*, that are also generally present in the data.

The assumption of a flat disc plane is equivalent to requiring constant  $i$  & PA *in resuri*, which is the usual practice, except that *velfit* has the further advantage that it determines the optimal values as part of the fit. The inner parts of spiral galaxy discs are believed to be flat: warps are generally observed to start near the edge of the optical disc (*e.g.* Briggs 1990) and theoretically we expect the massive inner disk to be coherent enough to resist bending (*e.g.* Shen & Sellwood 2006).

With the projection angles held at constant values for all radii, it may seem from Fig. 1 that fitting a simple circular flow model, *e.g.* with *rotcur*, would yield the same  $\bar{V}_t$  as a bisymmetric model from *velfit*. However, the estimated circular speeds for an axisymmetric model are biased towards values on the major axis where the line-of-sight component of the orbital motion is greatest. Since gas moving on elliptical orbits has its smallest orbital speed at apocentre,<sup>3</sup> the fitted  $\bar{V}_t$  is biased low when the streaming pattern is closely aligned with the major axis. Conversely, we should expect an axisymmetric fit to be biased high by the higher-than-average speed of the gas near pericentre when the bar is oriented close to the projected minor axis, and to yield a fair estimate of  $\bar{V}_t$  when the bar is at intermediate angles. Recall that  $\bar{V}_t$  is defined to be the average tangential velocity around a circle that may cross multiple streamlines, as shown in the strongly non-axisymmetric flow sketched in the upper panel of Fig. 1. Thus even though  $\bar{V}_t$  affords a fairer estimate of the central attraction than that from an

<sup>3</sup> Even in strong bars, where angular momentum is not approximately conserved, gas at apocentre of the stream lines must be moving slower than the average since it plunges inwards after that point, irrespective of the angular rotational speed of the potential that drives the non-circular flow.

axisymmetric fit, it is not the circular speed in the equivalent axisymmetric potential, unless the distortion is very mild.

Because *reswri* fits each ring independently, it is not easy to apply a smoothing constraint to the fit. Spiral arms, turbulence, *etc.*, produce localized distortions to the flow that can lead to “wiggles” in the fitted velocities, as well as small-scale variations in  $V_{\text{sys}}$ ,  $i$ , & PA. The user of *reswri* can, and probably should, hold these global parameters fixed, but the tool does not have the option to smooth the fitted velocities. While excessive smoothing is clearly dangerous, *e.g.* it could reduce the slope of the inner rotation curve, a small degree of smoothing applied to constrain the fit can be beneficial. In Appendix A we describe how an optional penalty can be applied within *velfit* to smooth the radial variations of the fitted functions  $\bar{V}_t(R)$ ,  $V_{m,t}(R)$ , &  $V_{m,r}(R)$ ; the magnitude of the penalty can be set independently for the axisymmetric and non-axisymmetric terms.

The tool *velfit* assumes a straight position angle for the non-axisymmetric distortion, which has both advantages and disadvantages. Since it cannot follow the radial winding of a spiral pattern, it “averages over” the spirals (advantage (iv) mentioned above) and fits only straight distortions with  $m$ -fold rotational symmetry. Its primary purpose therefore is to identify bar-like or oval distortions in the disk or halo. However, a fixed position angle precludes mapping the distorted flow of a spiral, which could be an interesting capability. It may be possible to adapt *velfit* to include extra parameters to fit a spiral of a certain shape, which we leave for possible future development.

A weakness of *velfit* is that it tends to return absurd velocities when the bar angle,  $\phi_b$ , is near zero or  $90^\circ$  because a degeneracy arises between the velocity components at these special orientations. To see this, consider equation (1) for the predicted projected velocity when  $\phi_b = 0$ : the products  $\cos 2\theta \cos \theta$  and  $\sin 2\theta \cos \theta$ , can be separated into a part that varies as  $\cos \theta$  and another that varies as  $\cos 3\theta$  or  $\sin 3\theta$ . Therefore  $\bar{V}_t$  is partly degenerate with both  $V_{2,t}$  and  $V_{2,r}$ , and a similar partial degeneracy arises when  $\phi_b = 90^\circ$ . In principle, the  $3\theta$  variation of the model breaks the degeneracy, but these more rapid angular variations are more susceptible to noise, and the “best fit” values of the three velocity components can be absurd. We show an example in section 4.4, where smoothing (Appendix A) proves valuable in controlling this numerical artefact.

The *velfit* code can be used to fit simultaneously for more than one type of distortion, but we have not obtained anything useful from attempting this. However, van de Ven & Fathi (2009) suspect both spiral perturbations and axisymmetric radial inflow in the central parts of NGC 1097, and fit for both using a generalization of the method proposed by Schoenmakers *et al.* (1997).

It should be noted that *velfit* is purely a fitting procedure. It does not, in general, yield a direct estimate of the potential responsible for the fitted velocity distortions, except when departures from axial symmetry are mild, as we show in the next section.

### 3 MILDLY DISTORTED POTENTIALS

Where the fitted non-circular speeds are a small fraction of the circular speed, we can use epicycle theory to relate the fitted non-circular velocities to the strength of the non-axisymmetric perturbation. We can use the formulae for the orbits of test particles on near circular orbits in weakly barred potentials from Binney & Tremaine (2008, hereafter BT08).<sup>4</sup> Their equation (3.147a, p190) gives the forced radial displacement as a function of time, which can easily be differentiated to find the forced radial speed. The radial velocity at radius  $R_0$  varies sinusoidally with amplitude

$$V_{m,r} = \left[ \frac{d\Phi_b}{dR} + \frac{2\Omega\Phi_b}{R(\Omega - \Omega_b)} \right]_{R_0} \frac{m(\Omega_0 - \Omega_b)}{\kappa_0^2 - m^2(\Omega_0 - \Omega_b)^2}, \quad (3)$$

where  $\Phi_b$  is the weak non-axisymmetric part of the potential that rotates at angular rate  $\Omega_b$ , and  $\Omega(R)$  &  $\kappa(R)$  are the usual frequencies of rotation and epicycle motion for mildly eccentric orbits. The time derivative of the equation for the tangential displacement (*e.g.* Sellwood & Wilkinson 1993, eq. 10b), converted to the same notation and abbreviating  $\omega = m(\Omega - \Omega_b)$ , gives

$$V_{m,t} = \left[ \frac{2\Omega}{\omega} \frac{d\Phi_b}{dR} + \frac{4\Omega^2 - \kappa^2 + \omega^2}{\omega^2} \frac{m\Phi_b}{R} \right]_{R_0} \frac{\omega_0}{\kappa_0^2 - \omega_0^2}. \quad (4)$$

With aspherical halos in mind, we simplify these general expressions for the case of a non-rotating potential distortion in a region where the rotation curve is approximately flat. (Other assumptions are possible, if desired.) Since we expect the halo to be rotating slowly, we assume  $\Omega_b \ll \Omega_0$ , we set  $\kappa_0^2 = 2\Omega_0^2$  for a flat rotation curve, and we assume the potential perturbation varies slowly with radius so that  $d\Phi_b/dR \ll \Phi_b/R$ . With these assumptions, choosing  $m = 2$  for a bisymmetric distortion and setting  $R_0\Omega_0 = V_c$ , equations (3) and (4) reduce to

$$V_{2,r} \simeq -\frac{2\Phi_b}{V_c}, \quad \& \quad V_{2,t} \simeq -\frac{3\Phi_b}{V_c}. \quad (5)$$

Thus if the perturbed velocities are caused by a weak, non-rotating, oval distortion to a quasi-logarithmic potential, we should expect the perturbed velocity coefficients to be in the ratio  $V_{2,t} \simeq 1.5V_{2,r}$  and, in particular, they should have the same sign. Note that we do not expect the perturbed coefficients to have this ratio when the oval distortion is strong and/or rapidly rotating, such as for bars, or in the inner parts where the rotation curve is rising.

In order to relate  $\Phi_b$  to the potential shape, we assume a non-axisymmetric potential of the form (*cf.* eq. 2.71a of BT08)

$$\Phi(R, \theta) = \frac{V_0^2}{2} \ln \left[ 1 + \frac{R^2}{R_c^2} \left( 1 + \frac{1 - q_\Phi^2}{q_\Phi^2} \sin^2 \theta \right) \right], \quad (6)$$

where  $V_0$  sets the velocity scale,  $R_c$  is the core radius, and  $q_\Phi$  is the axis ratio of the potential. In the limit of  $q_\Phi \lesssim 1$ , this is the potential of a mildly non-axisymmetric galaxy having flat outer rotation curve, of the kind we assumed above. Expansion of this potential for small  $(1 - q_\Phi^2)/q_\Phi^2$ , and comparison with the definition of  $\Phi_b$  in equations (3.136)

<sup>4</sup> Gas streamlines trace test particle orbits when pressure and magnetic forces can be neglected.

and (3.143) of BT08, we find  $\Phi_b = -V_c^2(1 - q_\Phi^2)/(4q_\Phi^2)$ . Combining this result with eq. (5) and equating  $\bar{V}_t$  to  $V_c$ , we finally obtain

$$q_\Phi = \left( \frac{\bar{V}_t}{\bar{V}_t + 2V_{2,r}} \right)^{1/2}. \quad (7)$$

We stress that this formula assumes a mildly distorted, slowly rotating potential and a flat rotation curve, and it will not yield a reliable estimate in other circumstances. As is well known, the density that gives rise to this potential is about three times more elongated than the potential, so that  $q_\rho \simeq 1 - 3(1 - q_\Phi)$  (BT08, p. 77).

## 4 RESULTS

Here we apply the tool *velfit* to several galaxies in the THINGS sample (Walter *et al.* 2008). The HI Nearby Galaxy Survey (THINGS) used the Very Large Array operated by the National Radio Astronomy Observatory<sup>5</sup> to make spectral observations of the 21cm line emission of neutral hydrogen in a sample of 34 galaxies. The data are in the public domain. We do not reanalyse the entire THINGS sample here, but choose a few representative galaxies to illustrate the advantages of *velfit* over *reswri*.

We selected data with natural weighting, which have higher signal-to-noise (S/N) and lower spatial resolution than when robust weighting is used, and downloaded maps of the intensity-weighted mean velocity. In order to apply a S/N cut-off, we also downloaded the data cubes. We determined the noise level,  $\sigma$ , from parts of channel maps with no signal, and discarded velocity measurements from the maps for which the peak intensity in any channel  $< 5\sigma$ .

The usual  $\chi^2$  function, defined in eq. (2), requires an estimate for the error  $\sigma_n$  in the data at each point in the map. Since the neutral hydrogen clouds in a galaxy have typical random velocities of 6-12 km s<sup>-1</sup> (Kamphuis 1993), we do not adopt the formal (generally much smaller) uncertainties in the intensity-weighted mean velocities, but instead assume a constant uncertainty of  $\sigma_n = 10$  km s<sup>-1</sup>. We have checked that our results are insensitive to values in the range  $\sigma_n = 10 \pm 4$  km s<sup>-1</sup>.

We choose the spacing between the rings in our model to be the beam width in order that each ring is independent. The beam size differs for each galaxy, ranging from 7.41'' for NGC 2976 to 15.6'' for NGC 7793. Since smoothing carries with it the danger that it may “smooth away” real features in the rotation curve, we do not employ it as a matter of routine. However, smoothing is essential to stabilize the fits to the data for NGC 2903, where the bar is close to the major axis (see §2).

We adopt the distances given in Table 1 of Walter *et al.* (2008) solely for the purpose of marking radii in kpc as well as in arcsec in the rotation curve plots.

### 4.1 Errors

Velocity residuals at each pixel have correlations due to features in the data, caused by spiral arms for example, that are not part of the fitted model. In addition, a small fraction of pixels have large residuals. These properties of the data, together with our use of arbitrary uncertainties, imply that the values on the  $\chi^2$  surface cannot be used to obtain error estimates on the parameters of the model.

We therefore adopt a bootstrap technique to estimate the true uncertainties in all fitted quantities, including the velocities. This standard non-parametric method (*e.g.* Chernick 1999) yields statistical uncertainties in fitted quantities without making assumptions about the underlying distribution of the residuals between the model and the data values. The spread of estimated quantities from repeated fits to resampled (or pseudo-)data yields an estimate of the true uncertainty. We give further details of our procedure in Appendix B.

The error bars on our velocity estimates, and the uncertainties in our tabulated values, are the rms variations of each quantity from 1000 bootstrap iterations. These statistical uncertainties reflect the peculiarities in the distribution of the errors in the data values, as well as some of the systematic inadequacies of the fitted model, which ignores features such as shocks or spiral streaming. They do not include possible systematic errors from other sources such as beam smearing or pressure support, neither can they reflect possible systematic differences between different data sets. As we report here, different kinematic data obtained from a different instrument, and perhaps arising from a different component of the ISM, can yield different estimates of the same physical quantities. A disagreement by more than the properly estimated errors is an indication either of systematic errors in one or both data sets or the inadequacy of the model.

### 4.2 NGC 2976: A Case Study

NGC 2976 is a nearby dwarf galaxy in the THINGS sample which was also studied in great detail by Simon *et al.* (2003). Velocity maps have therefore been made using the 21 cm line of HI, the optical H $\alpha$  emission lines, and the <sup>12</sup>CO( $J = 1 \rightarrow 0$ ) line. Clear distortions are visible in the velocity maps, indicating departures from a simple, coplanar axisymmetric flow.

Simon *et al.* (2003) fitted their data with a model that combined the usual circular flow pattern with an axisymmetric radial flow. SS07 found that an oval or bar-like distortion could yield an equally good fit to the same data. TBWBK find that a tilted ring model fits the HI data, which they conclude is consistent with tiny deviations from a round potential, albeit with a  $\lesssim 30^\circ$  variation in the inclination and a similar change of PA in the inner part of the galaxy.

Fig. 2(a) shows our fit to the same HI observations used by TBWBK when we assume a flat disc plane and fit for bisymmetric flows to  $R = 105''$  only. The residual velocities after subtracting our best fit model are typically less than 5 km/s, and fewer than 1% of the pixels have residuals larger than 20 km/s. The error bars show  $\pm\sigma$  uncertainties from the bootstrap analysis. de Blok *et al.* (2008) report a mild warp for  $R \gtrsim 125''$ , but we have excluded data at these

<sup>5</sup> NRAO is a facility of the National Science Foundation operated under cooperative agreement by Associated Universities Inc.

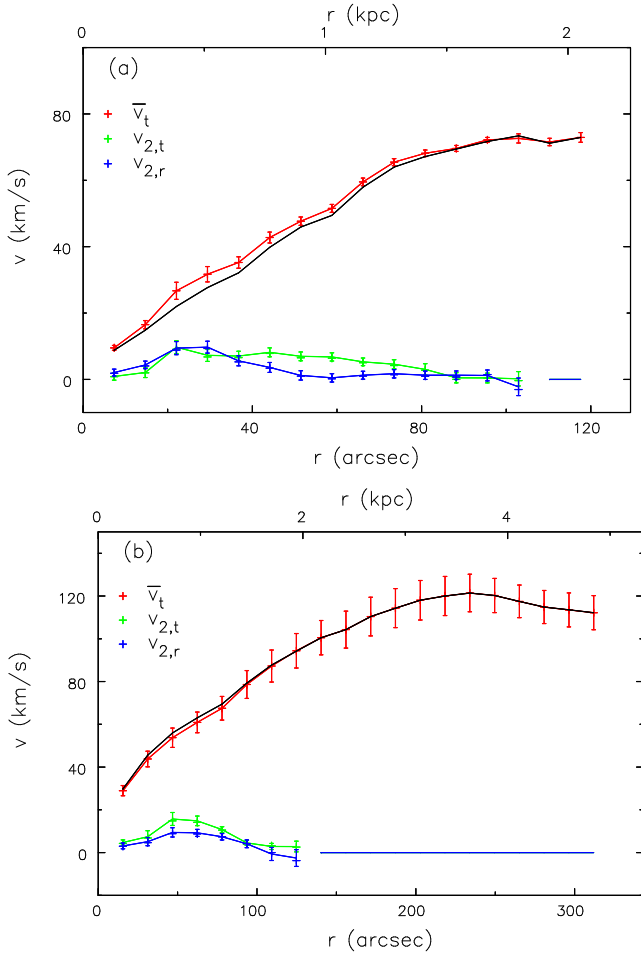


**Figure 2.** Our best fit rotation curve and streaming velocities derived using *velfit* on the THINGS data for (a) NGC 2976 and (b) NGC 7793. The black line shows the result of an axisymmetric fit to all radii and the error bars represent  $\pm\sigma$  uncertainties.

**Table 1.** Best-fit parameters for NGC 2976 and NGC 7793

	NGC 2976	NGC 7793
Adopted distance (Mpc)	3.6	3.9
Systemic vel. ( $\text{km s}^{-1}$ )	$1.6 \pm 0.1$	$226.9 \pm 0.1$
Disc inclination $i$	$61^\circ \pm 1^\circ$	$44^\circ \pm 5^\circ$
Disc PA, $\phi'_d$	$323^\circ \pm 1^\circ$	$292^\circ 0 \pm 0^\circ 4$
Bar axis $\phi_b$	$-29^\circ \pm 6^\circ$	$51^\circ \pm 8^\circ$
Projected bar axis $\phi'_b$	$308^\circ \pm 3^\circ$	$334^\circ \pm 7^\circ$

large radii because they have low S/N. While our estimate of PA (Table 1) is in good agreement with that derived from the same HI data by de Blok *et al.* (2008), our value of the inclination is somewhat lower than the  $i = 65^\circ$  they adopted, although their value is estimated from the restricted annular range  $80'' \leq R \leq 110''$ , whereas ours is from a global fit that includes bi-symmetric streaming over most of the disc.

We find (Fig. 2a) clear non-circular streaming motions in the inner galaxy in these HI data that are similar to, but of somewhat smaller magnitude than, those found by SS07 from the combined H $\alpha$  and CO data. Even though the perturbed velocities are  $\lesssim 10 \text{ km s}^{-1}$ , they are still a large enough fraction of the orbit speed that *velfit* is required;

notice that the black line, which shows  $V_c$  estimated in an axisymmetric fit such as would be found from *reswri*, is consistently lower than  $\bar{V}_t$ . We also find a smaller inclination angle than  $i \sim 64^\circ$  fitted by SS07. The origin of these differences, which are barely consistent within the quoted errors, is clearly due to fitting different datasets, with HI data arising from a different physical component.

We estimate the projected orientation of the bar or oval to be  $\phi'_b \simeq 308^\circ \pm 3^\circ$ , which is barely consistent with the  $\sim 315^\circ \pm 4^\circ$  estimated (from different data) by SS07. The difference in angles implies that the bar is slightly farther from the major axis, which in turn reduces the difference (Fig. 2a) between  $\bar{V}_t$  and the axisymmetric fit, for the reason given in section 2. Note, however, that we obtain a projected bar angle in closer agreement with that estimated by SS07 if we fix the galaxy inclination at their estimated value, indicating that the non-circular streaming motions in the neutral hydrogen arise from forcing by the same non-axisymmetric potential.

The probable reason that the bar streaming velocities we find here are weaker than those of SS07 is the significantly less pronounced ‘S’-shaped distortions of the velocity contours in the HI data (see Fig. 28 of TBWBK) than those shown in Fig. 2(a) of SS07. Since the distortions are well-resolved, it is unlikely that the differences result from the minor difference in spatial resolution of the two datasets: the beam-size of the HI data,  $7.41''$ , is  $\sim 50\%$  greater than the  $5''$  smoothing length adopted by Simon *et al.* (2003) for the combined CO and H $\alpha$  data used by SS07. (Note that Simon *et al.* (2003) show that velocity estimates from both CO and H $\alpha$  data, which are almost entirely from HII regions, are generally in good agreement with each other.) We can only speculate as to why the neutral hydrogen has milder non-circular motions than either the molecular or ionized gas; perhaps the HI layer has a greater physical thickness than the molecular/ionized layer and therefore greater ‘‘pressure’’ (in reality larger turbulent speeds), which causes a weaker response to a non-axisymmetric potential. Note that if the source of the non-axisymmetric potential is a bar in the disc of this galaxy, a thick gas layer will feel a weaker potential only if the bar is much thinner vertically than is the HI layer.

Since all three models, with radial flows (Simon *et al.* 2003), a twisted disc (TBWBK), or oval streaming (SS07 and Fig. 2a), are adequate fits to the data, there is no statistical reason to prefer one over another. However, the oval streaming model both avoids the ‘‘continuity problem’’ inherent in radial flow models, and also avoids a strong twist in the plane of the inner disc; TBWBK suggest the disc plane at  $R \sim 20''$  ( $\simeq 300 \text{ pc}$ ) is inclined to the plane of the main part of disc at  $R \sim 1.5 \text{ kpc}$  by  $\sim 30^\circ$ , while the light distribution does not give any indication of such an unusual feature.

### 4.3 Effects of bar orientation

The value of  $\bar{V}_t$  in Fig. 2(a), while smaller than obtained from different data by SS07, is higher than results from a purely axisymmetric flow fit, shown by the black line. The bisymmetric fitted  $\bar{V}_t$  is larger in this case because the ‘‘bar’’ is oriented such that its principal axis is not far from to the major axis of projection for the galaxy, as discussed in sec-

tion 2. We therefore also present a case where the bisymmetric fit has little effect on  $\bar{V}_t$ .

Fig. 2(b) shows a fit to the THINGS data for NGC 7793. As always, we attempt to fit only the flat part of the disc; in this galaxy, de Blok *et al.* (2008) find a mildly varying disc inclination over the entire radial range, but the PA clearly rises steadily for  $R \gtrsim 320''$ , which we tentatively interpret as the start of a warp. We fit a bisymmetric flow over the inner disk  $R < 125''$  only and an axisymmetric model to  $R = 320''$ . The best fit parameters and uncertainties are given in Table 1. Our best-fit  $i$  & PA are in good agreement with the values estimated by de Blok *et al.* (2008) from their tilted ring analysis.

The uncertainty in our estimate of the inclination is, however, rather larger than in other cases, possibly because of spiral streaming in the outer disc, which is not included in our model, or perhaps because the entire disk is warped, as suggested by TBWBK. Their explanation seems the more likely because the bootstrap values for this parameter have a distinctly bimodal distribution symmetrically distributed about the best-fit value; conservatively, we estimate the uncertainty from the rms spread of the bootstrap iterations. The uncertainty in the inclination is reflected in the uncertainties in the velocities, which therefore seem large relative to the smoothly varying means.

We find clear evidence (Fig. 2b) for non-circular streaming in the inner parts. Since we find  $\phi_b \simeq 49^\circ$ , the estimated “rotation curve” from the bisymmetric fit is in close agreement with that from the simple circular flow model, as expected from the discussion in section 2. TBWBK describe this galaxy as their best candidate for a non-axisymmetric potential in the *outer parts*, but they acknowledge that the problem of the apparent changing inclination complicates this interpretation. However, the more rapid radial changes in  $i$  & PA in the inner parts of their fits again appear to have masked the non-circular streaming we detect.

#### 4.4 Strong bars

TBWBK find non-circular motions that are consistent with a round potential in all the THINGS galaxies (their Table 3), despite the fact their sample contains several galaxies that are quite strongly barred. In these cases, however, the 21cm line emission from the barred region is generally too weak to yield reliable velocity estimates; velocities can be measured in limited patches in some cases, *e.g.* NGC 925, but not anywhere in others, *e.g.* NGC 3627. However, the data from NGC 2903 are good enough over almost the entire barred region ( $R \lesssim 60''$ ) to yield velocities above our S/N threshold. In this galaxy, TBWBK estimate the median value of  $m = 2$  streaming motions in the bar region is only  $\sim 14 \text{ km s}^{-1}$ , and conclude that the mean elongation of the overall potential is nevertheless consistent with being round.

The application of *velfit* to this galaxy presents a substantial challenge because the bar is so closely aligned with the major axis of projection. As discussed in section 2, the velocities  $\bar{V}_t$ ,  $V_{2,t}$  &  $V_{2,r}$  become harder to distinguish as  $|\phi_b| \rightarrow 0$ , and *velfit* can return unphysically large values for all ( $\gg 1000 \text{ km s}^{-1}$  in magnitude), even though they still fit the data well when combined as eq. (1). We overcome this problem to a large extent by applying a very small

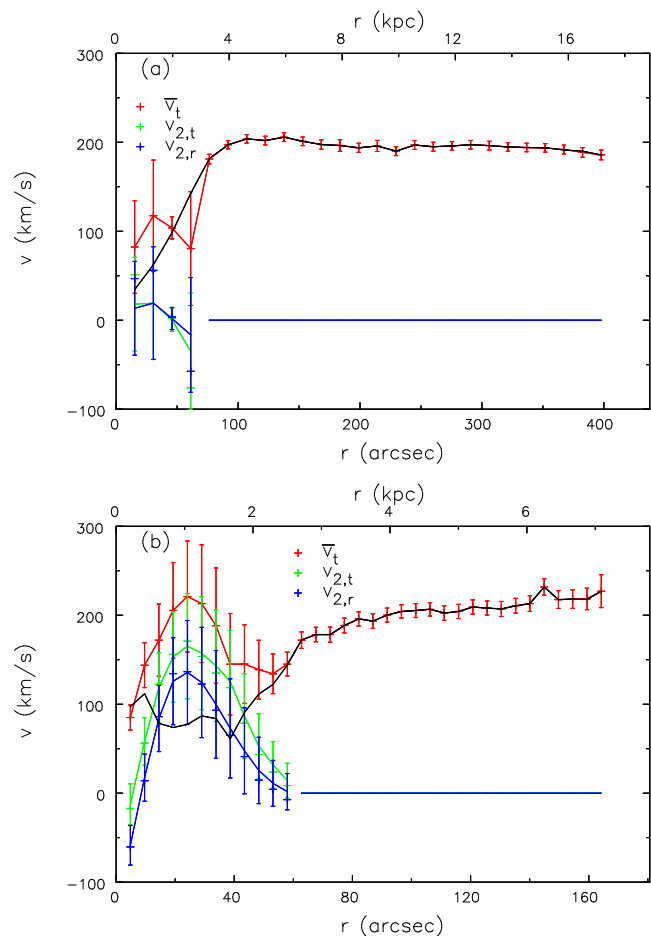


**Figure 3.** Our best fit rotation curve and streaming velocities derived for NGC 2903 using *velfit* on (a) the THINGS data and (b) the BH $\alpha$ Bar data – note the different scales.

**Table 2.** Best-fit parameters for NGC 2903

	THINGS data	BH $\alpha$ Bar data
Adopted distance (Mpc)	8.9	
Systemic vel. ( $\text{km s}^{-1}$ )	$549.9 \pm 0.3$	$554.1 \pm 0.5$
Disc inclination $i$	$64^\circ \pm 1^\circ$	$66^\circ \pm 3^\circ$
Disc PA, $\phi'_d$	$201.5 \pm 0.5$	$204^\circ \pm 1^\circ$
Bar axis $\phi_b$	$6^\circ \pm 14^\circ$	$-12^\circ \pm 8^\circ$
Projected bar axis $\phi'_b$	$204^\circ \pm 6^\circ$	$199^\circ \pm 4^\circ$
Smoothing penalty, $\lambda$	$1.7 \times 10^{-4}$	$6.6 \times 10^{-5}$

smoothing penalty, as described in Appendix A. Fig.3(a) shows the results from *velfit* applied to the THINGS data for  $R < 400''$ ; the parameters of this fit are given in Table 2 for  $\lambda = 1.7 \times 10^{-4}$ , but results are insensitive to variations of a factor of a few about this value.<sup>6</sup>

The smoothing penalty successfully eliminates absurd velocities in the bar region obtained from the bootstrap analysis, but at the cost of introducing a strong bias against finding  $|\phi_b| \lesssim 2^\circ$ . The reason appears to be a ridge in the  $\chi^2$  surface as  $\phi_b \rightarrow 0$  caused by the smoothing penalty, which disfavours the wildly varying velocities that would achieve the

<sup>6</sup> This apparently bizarre choice is  $\lambda = 0.002/\mathcal{A}$  for  $V_{\text{typ}} = 200 \text{ km s}^{-1}$ ; see Appendix A.

smallest residuals. We therefore prefer a very small smoothing penalty since larger values widen the range of disfavoured bar angles even though they further reduce the scatter of fitted velocities from the bootstrap iterations. On the other hand, increasing the smoothing penalty 50-fold, leads to an almost linear rise in  $\bar{V}_t$ , even for the bisymmetric fit, which illustrates the perils of oversmoothing.

Our best-fit estimate of the bar angle is  $\phi_b \sim 6^\circ$ . It should be noted that neither this angle, nor the best fit values of  $\bar{V}_t$  change significantly when we eliminate the smoothing penalty altogether.

Our fitted values of  $i$  & PA are in good agreement with those estimated by de Blok *et al.* (2008), and their rotation velocities are in good agreement with our axisymmetric fit, the black line in Fig. 3(a), that rises in a quasi-linear fashion from the origin. Naturally, they find wildly varying values of both  $i$  and PA in their innermost few rings, whereas *velfit* requires a flat plane and consequently our bisymmetric fit (red line) finds different velocities in this region. We find somewhat larger non-circular speeds in the bar region than those estimated by TBWBK, although the uncertainties in our estimates also are large enough that a round potential could not be excluded. Thus, the surprisingly weak bar streaming motions are not merely an artefact of *reswri*.

Since the beam width of the HI data we fit is  $\sim 15''$  (equal to our ring spacing in *velfit*) and the bar semi-axis is about four beam widths, it is likely that the HI data is not fully able to resolve the bar flow.<sup>7</sup> Fortunately, the velocity field of this galaxy has also been mapped at higher spatial resolution in the  $^{12}\text{CO}(J = 1 \rightarrow 0)$  line (Helfer *et al.* 2003) and in H $\alpha$  using a Fabry-Pérot instrument (Hernandez *et al.* 2005). We here show fits to the H $\alpha$  data (kindly made available by Olivier Hernandez) since they extend to larger radii than do the CO data, albeit with lower spatial resolution (4.8'').

Fig. 4(a) shows a 2MASS<sup>8</sup> H-band image of the galaxy, together with (b) the velocity map from the BH $\alpha$ Bar survey, (c) our best fit model and (d) & (e) residuals from an axisymmetric and full bar flow fits.

Table 2 and Fig. 3(b) give the results we obtained from by applying *velfit* to the H $\alpha$  data for NGC 2903 – note that the radial scales in panels (a) & (b) of Fig. 3 differ. We used a similar smoothing ( $\lambda = 6 \times 10^{-5}$  in this case) in order to eliminate absurdly large velocities in the bootstrap analysis, which introduces a bias, as before, against bar angles close to zero; since this bias causes a strong skewness in the distribution of bar angles, we estimated the uncertainty in this quantity from only those values more negative than the best fit value. The parameters of the fit to these data are generally in good agreement with those from the HI data, and the projected bar angles differ within their uncertainties.

However, the H $\alpha$  data show a much more pronounced

non-circular flow pattern within the bar region ( $R \lesssim 60''$ ), with perturbed velocities almost as large as  $\bar{V}_t$ , which in turn significantly exceeds the estimated circular speed from an axisymmetric fit to the same data (black line) and the derived  $\bar{V}_t$  from the HI data. The fitted velocities from the two datasets are in reasonable agreement outside the bar region, for as far as the optical data extend. The uncertainties in the bar region are still large, and significantly larger than the point to point variation in the best fit suggesting that slightly more aggressive smoothing could be warranted.

Thus it is clear that inadequacies in the HI data are the reason TBWBK concluded that non-circular motions within the bar were small. While the beam size of the THINGS data is not fully adequate to resolve the bar flow, the general paucity of neutral gas in the barred regions of other galaxies suggests it is also likely that HI is simply not a faithful tracer of the bar flow. Data from a different component of the ISM having better spatial resolution and fuller spatial coverage do reveal a pronounced non-circular streaming pattern, as expected for this strongly barred galaxy.

#### 4.5 Searching for Aspherical Halos

We here attempt to constrain the shapes of dark matter halos by searching for non-circular streaming motions in the outer discs of the THINGS sample. Since the current version of *velfit* assumes the galaxy plane to be flat, it cannot be used in warped regions, which generally arise outside the visible disc. We are therefore restricted to just two galaxies in the sample, NGC 3198 & NGC 2403, for which the extended HI disc is known from the analysis of de Blok *et al.* (2008) to be approximately coplanar with the inner disc.

Even though these two galaxies are not strongly warped, the analysis of TBWBK, which allows changes in PA and  $i$  from ring to ring, may underestimate the ellipticity of the dark matter halos in the disc plane. However, the main advantage of *velfit* over *reswri* in these circumstances is that it searches for a bisymmetric distortion that is coherent over a wide range of radii and could, in principle, detect very mild distortions that might be masked by various sources of noise, such as turbulence and local spiral streaming. Since it is a more sensitive probe of halo shapes, it should either detect mild distortions, if they are present, or place a tighter lower bound on the axis ratio of the potential.

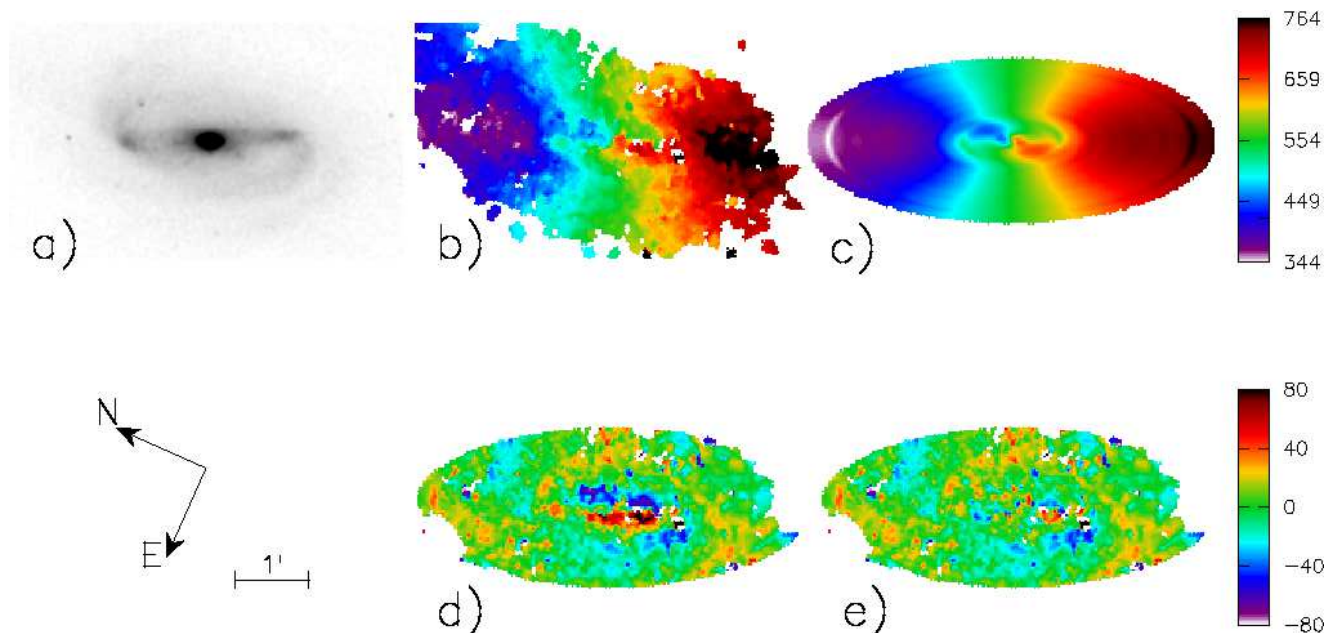
##### 4.5.1 NGC 3198

Fig. 5 shows the residual map to  $R = 456''$  when a flat, axisymmetric model is subtracted from the THINGS data for NGC 3198. The residual velocities are generally small, peaking at  $\pm 20 \text{ km s}^{-1}$ , which is consistent with the small variations in  $i$  & PA for  $r > 200''$  reported by de Blok *et al.* (2008). However, the residual pattern reveals clear indications of mild spiral arm streaming, even far outside the optical disc ( $R_{25} \simeq 255''$  in the B-band, de Vaucouleurs *et al.* 1991).

In order to search for a possible mildly non-axisymmetric halo, we tried fitting a bisymmetric model, with no spirality, to the outer disc. Such a model may be able to identify a weak bar flow that could be buried in the spiral noise. The parameters of our best fit model, which

<sup>7</sup> Robust weighting of HI data yields velocity maps with higher spatial resolution but lower S/N. For NGC 2903, however, these data from the bar region have too low S/N to allow meaningful fits.

<sup>8</sup> Atlas Image obtained as part of the Two Micron All Sky Survey (2MASS), a joint project of the University of Massachusetts and the Infrared Processing and Analysis Center/California Institute of Technology, funded by the National Aeronautics and Space Administration and the National Science Foundation.



**Figure 4.** (a) An H-band image of NGC 2903 from 2MASS (Skrutskie *et al.* 2006). (b) The velocity map made using the H $\alpha$  line (Hernandez *et al.* 2005). (c) Our best fit model with a bar flow. (d) Residuals after subtracting the best fit axisymmetric model – note the large values in the bar region. (e) Residuals after subtracting our best fit bi-symmetric flow model. The velocity scales to the right are in km s $^{-1}$ ; all images have the same orientation and spatial scale, indicated by the 1' scale bar.

**Table 3.** Best-fit parameters for NGC 3198 and NGC 2403

	NGC 3198	NGC 2403
Adopted distance (Mpc)	13.8	3.2
Systemic vel. (km s $^{-1}$ )	$660.2 \pm 0.3$	$133.5 \pm 0.3$
Disc inclination $i$	$70^\circ.4 \pm 0^\circ.3$	$64^\circ \pm 1^\circ$
Disc PA, $\phi'_d$	$216^\circ.2 \pm 0^\circ.5$	$123^\circ.8 \pm 0^\circ.6$
Bar axis $\phi_b$	$46^\circ \pm 14^\circ$	$296^\circ \pm 12^\circ$
Projected “bar” axis $\phi'_b$	$236^\circ \pm 5^\circ$	$82^\circ \pm 5^\circ$

includes a bisymmetric flow for  $R \gtrsim 220''$ , are listed in Table 3. Our estimated values of  $V_{\text{sys}}$ ,  $i$ , & PA are in excellent agreement with those given by de Blok *et al.* (2008).

Fig. 6 shows that the best fit non-axisymmetric velocities are no larger than  $\sim 6\%$  of the circular speed and vary slowly with radius. If the perturbed velocities are caused by a slowly-rotating, mild oval distortion of the halo in the outer parts where the rotation curve is approximately flat, we should observe  $V_{2,t} \simeq 1.5V_{2,r}$  (eq. 5). In fact, the coefficients are not in this predicted ratio at any radius and even the signs differ over the inner part of the fitted range suggesting a different origin for the perturbed velocities, such as spiral arm streaming for which a fixed axis and slow rotation for the perturbation are inappropriate assumptions. Our fitted values of  $\phi_b$ ,  $V_{2,t}(R)$ , and  $V_{2,r}(R)$  are merely those that achieve the largest reduction in  $\chi^2$  from the residual pattern shown in Fig. 5. In particular, the PA of the fitted “bar” varies with radius as we sub-divide the fitted region, as one would expect if the fit is picking up different fragments of the spirals.

Thus we are unable to identify a velocity pattern indicative of a non-axisymmetric halo. Whatever possible halo distortion may be present, it is clearly still weaker than the mild spiral features we do detect. We therefore concur with

TBWBK that the data from NGC 3198 are consistent with this galaxy living in a perfectly round halo.

Even though we do not have a firm detection of a bar-like distortion in the halo, we can use the results in Fig. 6 to place a lower bound on its ellipticity by making a rough estimate of the maximum halo distortion that could be masked by the spiral contribution. We therefore suppose that the disturbed velocities are due to a combination of a slightly elongated halo and a spiral disturbance in the disc plane. In this situation, the variation of the total amplitude of the velocity distortions will be modulated by the changing angle between the two as the phase of the spiral changes with radius; it will be a maximum when the distortions are aligned and a minimum when they are perpendicular. (This is a conservative assumption, since amplitude and phase variations could also be caused by the changing distance from a resonance in just a single spiral, with no second component of the disturbance potential.)

For NGC 3198, the combination  $A_{\text{tot}} = (V_{2,r}^2 + V_{2,t}^2)^{1/2}$  varies from a minimum of  $A_{\text{tot}} = 1.25 \text{ km s}^{-1}$  at  $296''$  to  $A_{\text{tot}} = 11.10 \text{ km s}^{-1}$  at  $444''$ . If this spans a full range of possible phase differences ( $0$  to  $\pi/2$ ), and the spiral and halo contributions are separately roughly constant, then  $A_{\text{tot}} = A_s + A_h$  at maximum, and  $A_{\text{tot}} = A_s - A_h$  at minimum. Solving for the separate spiral and halo amplitudes, we find  $A_s \simeq 6.3 \text{ km s}^{-1}$  and  $A_h \simeq 5.0 \text{ km s}^{-1}$ . Since  $V_{2,t} = 1.5V_{2,r}$  for a mild, non-rotating distortion with a flat rotation curve (eq. 5), we expect  $V_{2,r} \simeq A_h/1.8$ . Using the values  $V_{2,r} \simeq 5/1.8 \text{ km s}^{-1}$  and  $\bar{V}_t = 140 \text{ km s}^{-1}$  in formula (7), we find  $q_\Phi \gtrsim 0.98$  and  $q_\rho \gtrsim 0.94$  as our estimated lower limits on the axis ratios of the potential and density of the halo in NGC 3198.

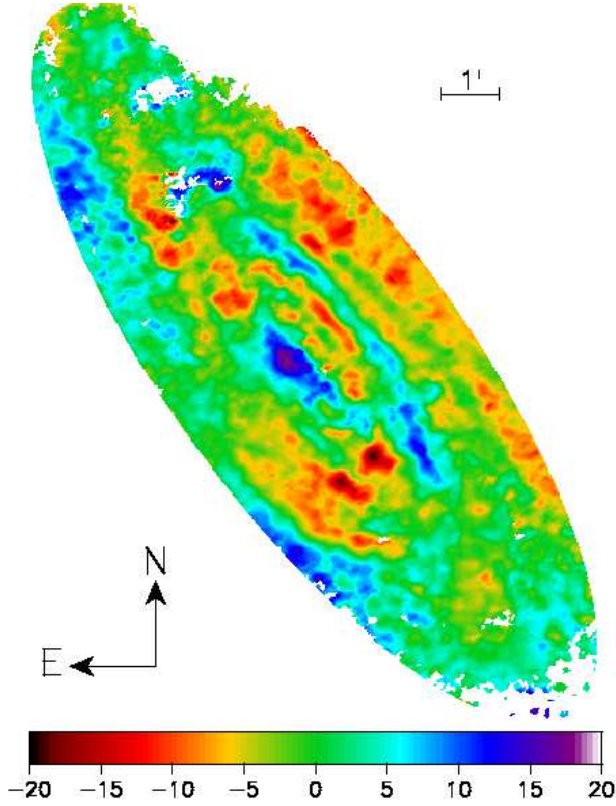


**Figure 5.** Residuals after fitting an axisymmetric model to the THINGS data for NGC 3198. The outer ellipse has a semi-major axis of  $r = 456''$  and velocities in the colour bar are in  $\text{km s}^{-1}$ .

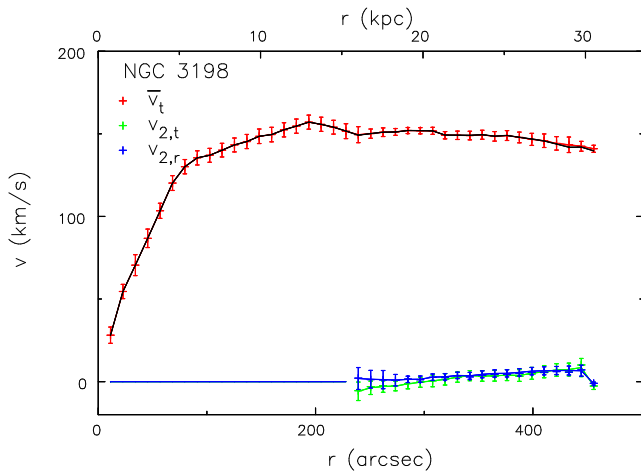


**Figure 6.** Results from *velfit* using THINGS data for NGC 3198. The black line shows the result of an axisymmetric fit to all radii, while the coloured points show  $\bar{V}_t(R)$  (red),  $V_{2,t}(R)$  (green), &  $V_{2,r}(R)$  (blue) from a bisymmetric fit restricted to the range  $240'' \leq R \leq 460''$  with an axisymmetric model fitted to other radii.

#### 4.5.2 NGC 2403

Fig. 7 shows that a simple, flat, axisymmetric model is a good fit to the THINGS data for NGC 2403, consistent with the tiny variations in  $i$  & PA reported by (de Blok *et al.* 2008). The small residuals are somewhat less indicative of

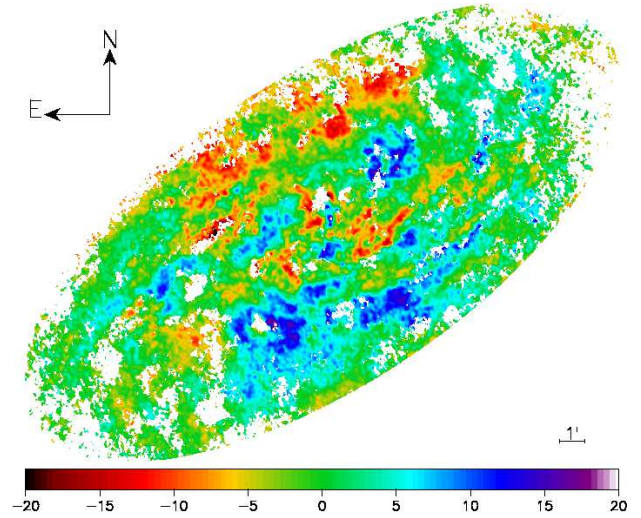


**Figure 7.** Residuals after fitting an axisymmetric model to the THINGS data for NGC 2403. The outer ellipse has a semi-major axis of  $r = 844''$  and velocities in the colour bar are in  $\text{km s}^{-1}$ .

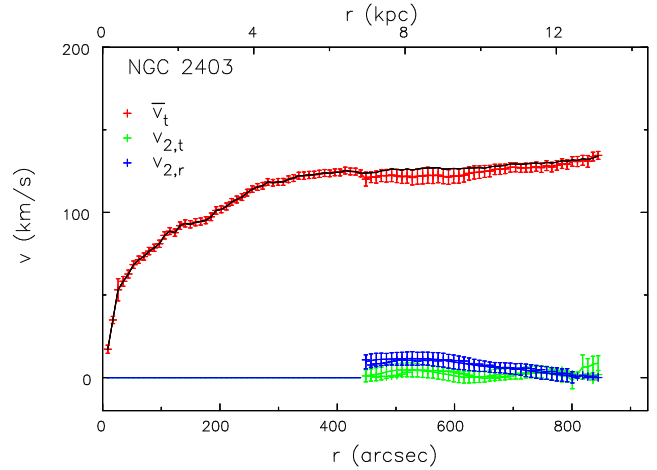


**Figure 8.** Same as for Fig. 6 but for NGC 2403.

spiral streaming than in NGC 3198, and show hints of a more global N-S anti-symmetry at larger projected radii ( $R_{25} \simeq 656''$  in the B-band de Vaucouleurs *et al.* 1991).

Our fitted values of  $V_{\text{sys}}$ ,  $i$  & PA from a model that includes bisymmetric streaming velocities for  $R > 450''$ , listed in Table 3, are in excellent agreement with those found by de Blok *et al.* (2008). Fig. 8 shows that the perturbed velocities are  $\lesssim 10 \text{ km/s}$ , but the radial component is generally the larger, which is inconsistent with a non-rotating, bar-like distortion. Thus we again concur with TBWBK that the THINGS data on this galaxy are consistent with it living in a perfectly round halo.

While the perturbed velocities are not of the form expected for a mild, non-rotating halo distortion, we proceed as for NGC 3198. For NGC 2403, we find  $A_{\text{tot}}$  varies from a maximum of  $A_{\text{tot}} = 11.86 \text{ km s}^{-1}$  at  $510''$  to  $A_{\text{tot}} = 2.12 \text{ km s}^{-1}$  at  $809''$ . Again assuming this spans a full range of possible phase differences and the spiral and halo contributions are separately roughly constant, then  $A_s \simeq 7.0 \text{ km s}^{-1}$  and  $A_h \simeq 4.9 \text{ km s}^{-1}$ . Using the values

$V_{2,r} \simeq 4.9/1.8 \text{ km s}^{-1}$  and  $\bar{V}_t = 120 \text{ km s}^{-1}$  in formula (7), we again find  $q_\Phi \gtrsim 0.98$  and  $q_\rho \gtrsim 0.94$  as our estimated lower limits on the axis ratios of the potential and density of the halo in NGC 2403.

## 5 CONCLUSIONS

Spekkens & Sellwood (2007) devised the software tool *velfit*, for fitting non-circular streaming flows in galaxies caused by non-spiral like distortions. We have shown here that it is altogether superior to the commonly used *reswri* (Schoenmakers *et al.* 1997). This is because it provides a correction for the systematic error in the azimuthally averaged orbital speed, it can fit strong distortions, it is more sensitive to radially coherent disturbances, it readily allows radial smoothing of the fitted velocities, and the estimated disturbed velocities are more easily related to the potential distortion. We also argue that while the current version of *velfit* assumes a flat plane for the inclined disc, this is no more restrictive, since tilts of individual rings in the bright inner part of the disk, as *reswri* allows, are dangerous and can lead to severe underestimation of the distorted velocities. This paper illustrates these advantages for a number of galaxies.

We show that the THINGS data (Walter *et al.* 2008) for NGC 2976 can indeed be fitted by an inner bar-like distortion, albeit somewhat milder than that found by SS07 from H $\alpha$ +CO data. We argue that a bar flow is more natural than either the radial flow fitted by Simon *et al.* (2003) or the twisted disk model of Trachternach *et al.* (2008). As shown in SS07, the improved mean orbital speed of the gas estimated from *velfit* is a fairer estimate than the simple mean fitted by tools such as *reswri*. The difference, which arises from the bias to the velocity on the major axis, can be of either sign depending on the orientation of the bar to the major axis of projection.

We also show that neutral hydrogen observations are not well suited to tracing gas dynamics in strongly barred potentials. The neutral hydrogen generally has a low column density in the barred region, and the velocity maps are generally too noisy or sparsely sampled to yield a clear indication of bar flow. Smoothing to lower spatial resolution improves signal-to-noise, and yields an almost fully sampled velocity map throughout the bar region of NGC 2903. We identify an oval flow pattern in these data of about the right physical size and with significant streaming velocities, but the large uncertainties imply they are also consistent with a round potential. However, a strong bar flow is unambiguously detected in our fit to the H $\alpha$  velocity map of Hernandez *et al.* (2005). While the superior spatial resolution of the optical data is clearly important, the generally patchy and faint emission from neutral hydrogen in the barred regions of this and other barred galaxies in the THINGS sample suggest that neutral hydrogen is simply a poor tracer of bar flows.

Our analysis of the THINGS data for NGC 3198 & NGC 2403 reaches a similar conclusion to that of TBWBK: that the halos of these two galaxies are close to round. Jog (2000) and Bailin *et al.* (2007) show that the self-consistent response of the disc can mask a large part of the distortion in the halo, but only when the disc is massive. In these

two cases, the outer gas disc probably has little mass and therefore could not hide a more substantial halo distortion.

However, it is hard to confront this result with the predictions of LCDM (cited in the introduction): not only is it based on just two galaxies, but it is possible these two galaxies are unrepresentative perhaps because only galaxies with unusually round halos could host an extensive disc of gas that is not warped! Clearly, measurements of halo shapes in a representative galaxy sample will require a tool that can reliably measure potential distortions in warped discs; we leave development of such a capability for future work. Other statistical approaches (Franx & de Zeeuw 1992; Trachternach *et al.* 2009) do, however, place some reasonably tight constraints on halo shapes.

Thus, while we confirm the conclusion of TBWBK that many galaxies in the THINGS sample have at most minor departures from axial symmetry, *velfit* reveals that mild bars are present in NGC 2976 and NGC 7793. We also show that a pronounced non-axisymmetric flow is revealed more clearly in other data for the strongly barred galaxy NGC 2903.

Another valuable application for *velfit* will be a preliminary analysis of the velocity maps of strongly barred galaxies. It would be very helpful to obtain a clear indication of whether the flow pattern is, or is not, well enough sampled and sufficiently regular to yield a result, before embarking on laborious mass modeling by the method described by Weiner *et al.* (2001). Furthermore, such a study needs approximate axisymmetric mass models, and the estimates of  $\bar{V}_t$  from *velfit* will be more useful than the ‘‘circular speed’’ estimated from other less powerful tools.

## ACKNOWLEDGMENTS

We thank Claude Carignan and Olivier Hernandez for supplying Fabry-Pérot maps of several galaxies from their BH $\alpha$ Bar survey. We also thank Andrew Baker, Ted Williams, and especially Tad Pryor for discussions. Kristine Spekkens, Jack Hughes, and an anonymous referee provided comments that have helped us to improve the paper. This work was supported by NSF grant AST-0507323.

## REFERENCES

- Allgood, B., Flores, R. A., Primack, J. R., Kravtsov, A. V., Wechsler, R. H., Faltenbacher, A. & Bullock, J. S. 2006, *MNRAS*, **367**, 1781
- Bailin, J., Simon, J. D., Bolatto, A. D., Gibson, B. K. & Power, C. 2007, *ApJ*, **667**, 191
- Begeman, K. G. 1987, PhD. thesis, University of Groningen
- Binney, J. & Tremaine, S. 2008, *Galactic Dynamics* 2nd edition (Princeton: Princeton University Press)
- Bosma, A. 1978, PhD. thesis, University of Groningen
- Briggs, F. H. 1990, *ApJ*, **352**, 15
- Chernick, M. R. 1999, *Bootstrap Methods: A Practitioner’s Guide* (New York: Wiley)
- Debattista, V. P., Moore, B., Quinn, T., Kazantzidis, S., Maas, R., Mayer, L., Read, J. & Stadel, J. 2008 *ApJ*, **681**, 1076
- de Blok, W. J. G., Walter, F., Brinks, E., Trachternach, C., Oh, S-H. & Kennicutt, R. C. 2008, *AJ*, **136**, 2648

- de Vaucouleurs, G., de Vaucouleurs, A., Corwin, H. G., Jr., Buta, R. J., Paturel, G., & Fouqué, P. 1991, Third Reference Catalogue of Bright Galaxies (New York: Springer)
- Dubinski, J. 1994, *ApJ*, **431**, 617
- Fathi, K.; van de Ven, G.; Peletier, R. F.; Emsellem, E.; Falcón-Barroso, J.; Cappellari, M. & de Zeeuw, T. 2005, *MNRAS*, **364**, 773
- Franx, M. & de Zeeuw, T. 1992, *ApJL*, **392**, L47
- Franx, M., van Gorkom, J. H. & de Zeeuw, T. 1994, *ApJ*, **436**, 642
- Hayashi, E. & Navarro, J. F. 2006, *MNRAS*, **373**, 1117
- Hayashi, E., Navarro, J. F. & Springel, V. 2007, *MNRAS*, **377**, 50
- Helfer, T. T., Thornley, M. D., Regan, M. W., Wong, T., Sheth, K., Vogel, S. N., Blitz, L. & Bock, D. C.-J. 2003, *ApJS*, **145**, 259
- Hernandez, O., Carignan, C., Amram, P., Chemin, L. & Daigle, O., 2005, *MNRAS*, **360**, 1201
- Jing, Y. P. & Suto, Y. 2002, *ApJ*, **574**, 538
- Jog, C. J. 2000, *ApJ*, **542**, 216
- Kamphuis, J. 1993, PhD. thesis, University of Groningen
- Kranz, T., Slyz, A. D. & Rix, H.-W. 2003, *ApJ*, **586**, 143
- Oh, S.-H., de Blok, W. J. G., Walter, F., Brinks, E. & Kennicutt, R. C. 2008, *AJ*, **136**, 2761
- Pence, W. D. & Blackman, C. P. 1984, *MNRAS*, **210**, 547
- Pérez, I., Fux, R. & Freeman, K. 2004, *A&A*, **424**, 799
- Schoenmakers, R. 1999, PhD. thesis, University of Groningen
- Schoenmakers, R. H. M., Franx, M. & de Zeeuw, P. T. 1997, *MNRAS*, **292**, 349
- Sellwood, J. A. & Wilkinson, A. 1993, *Rep. Prog. Phys.*, **56**, 173
- Shen, J. & Sellwood, J. A. 2006, *MNRAS*, **370**, 2
- Simon, J. D., Bolatto, A. D., Leroy, A. & Blitz, L. 2003, *ApJ*, **596**, 957
- Skrutskie, M. F. *et al.* 2006, *AJ*, **131**, 1163
- Sofue, Y. & Rubin, V. 2001, *ARAA*, **39**, 137
- Spekkens, K. & Sellwood, J. A. 2007, *ApJ*, **664**, 204 (SS07)
- Trachternach, C., de Blok, W. J. G., Walter, F., Brinks, E. & Kennicutt, R. C. 2008, *AJ*, **136**, 2720
- Trachternach, C., de Blok, W. J. G., McGaugh, S. S., van der Hulst, J. M. & Dettmar, R.-J. 2009, arXiv:0907.5533
- Valenzuela, O., Rhee, G., Klypin, A., Governato, F., Stinson, G., Quinn, T. & Wadsley, J. 2007, *ApJ*, **657**, 773
- van de Ven, G. & Fathi, K. 2009, arXiv:0905.3556
- van den Bosch, F. C. & Swaters, R. A. 2001, *MNRAS*, **325**, 1017
- van Eymeren, J., Trachternach, C., Koribalski, B. S. & Dettmar, R.-J. 2009, arXiv:0906.4654
- Walter, F., Brinks, E., de Blok, W. J. G., Bigiel, F., Kennicutt, R. C., Thornley, M.D. & Leroy, A. K. 2008, *AJ*, **136**, 2563
- Weiner, B. J. 2004, in *IAU Symp. 220, Dark Matter in Galaxies*, ed. S. Ryder, D. J. Pisano, M. Walker & K. C. Freeman (Dordrecht: Reidel), p. 35
- Weiner, B. J., Sellwood, J. A. & Williams, T. B. 2001, *ApJ*, **546**, 931
- Zánmar Sánchez, R., Sellwood, J. A., Weiner B. J. & Williams, T. B. 2008, *ApJ*, **674**, 797

## APPENDIX A: APPLYING A SMOOTHING PENALTY

The usual  $\chi^2$  function is defined in eq. (2), but we can minimize a new function if we wish

$$X^2 = \chi^2 + \lambda \sum_{k=2}^{K-1} \mathcal{A} [V_{k-1} - 2V_k + V_{k+1}]^2, \quad (\text{A1})$$

which adds a penalty for large second differences between the tabulated values  $V_k$ , which are assumed to be equally spaced. The constant  $\mathcal{A}$ , defined below, has dimensions of inverse square velocity in order to fulfil the requirement that the smoothing penalty be dimensionless. The value of the smoothing parameter,  $\lambda$ , which can be set independently for the axisymmetric and non-axisymmetric terms, can be adjusted as desired; small values have slight effect, while large values make the profile very smooth. Over-smoothing not only increases the value of  $\chi^2$ , but may reduce the inner slope and smooth other real features in the rotation curve.

Since the magnitude of the second velocity difference (in square brackets) varies as the inverse square of the ring spacing,  $\Delta R = R_{\text{max}}/N_R$ , we choose  $\mathcal{A} = (R_{\text{max}}/\Delta R)^4/V_{\text{typ}}^2 = N_R^4/V_{\text{typ}}^2$ , which ensures that the smoothing constraint is unaffected when the ring spacing is changed. Here,  $V_{\text{typ}}$  is a constant that is a rough estimate of a typical orbital speed in the disc.

The smoothness constraint is applied only in the matrix that is solved to find the optimal values for  $V_k$  (see SS07), and adds extra terms as follows:

$$\frac{\partial X^2}{\partial V_j} = \frac{\partial \chi^2}{\partial V_j} + 2\lambda \mathcal{A} (V_{j-2} - 4V_{j-1} + 6V_j - 4V_{j+1} + V_{j+2}). \quad (\text{A2})$$

## APPENDIX B: BOOTSTRAP ESTIMATION OF ERRORS

The bootstrap uses the spread of estimated quantities from repeated fits to resampled (or pseudo-)data to yield a non-parametric estimate of the true uncertainty in each quantity. To construct one realization of pseudo-data, we add to the predicted velocity from the best-fit model at every pixel a residual velocity from some other pixel chosen at random from residuals between the best fit model and the real data. Completely random resampling of residuals assumes that the residuals are uncorrelated, whereas inspection of our residual images generally reveals coherent patterns of residual velocities due to features, such as other forms of non-axisymmetric streaming and large-scale turbulence, which are not included in our fitted model. Pseudo-data constructed by fully random interchange eliminates correlations between the residuals and generally leads to unrealistically small uncertainties. Thus we require a scheme that will reproduce appropriately correlated errors at random at each iteration of the bootstrap.

Spekkens & Sellwood (2007) adopted constant residuals over small patches of the image, which worked well for the small galaxy NGC 2976 where most of the correlations appeared to arise from turbulence. But that scheme cannot capture the patterns of residuals that arise from spirals and other non-axisymmetric distortions that are clear features

in the residuals for larger galaxies. We therefore adopt a different approach here.

Since the dominant residual correlations appear over azimuthally extended regions in the disc plane, we manipulate the actual residual pattern as follows: we deproject it to face on and then, at every iteration, we rotate the residuals through a random angle. We also shift the residual pattern outwards by adding a constant to the radius of every pixel and subtract the maximum radius from those pixels that are shifted outside the map so that they fill the hole created in the centre by the outward shift. The constant used to shift in radius is a randomly-chosen fraction of the radius of the map. We then reproject the new residual pattern, and assign a residual velocity at each pixel in the pseudo-data from that of the nearest pixel in the scrambled residual image.

When we fit for an axisymmetric model in part of the galaxy and include a non-axisymmetric perturbation over a limited radial region, we scramble the residuals within each of these parts separately, and do not interchange residuals between the separate regions, since the appearance of residual patterns in the two regions can differ quite markedly.